nature neuroscience

Opioid inhibition of N-type Ca^{2+} channels and spinal analgesia couple to alternative splicing

Arturo Andrade[1,2], Sylvia Denome[1,2], Yu-Qiu Jiang[1], Spiro Marangoudakis[1] & Diane Lipscombe[1]

Alternative pre-mRNA splicing occurs extensively in the nervous systems of complex organisms, including humans, considerably expanding the potential size of the proteome. Cell-specific alternative pre-mRNA splicing is thought to optimize protein function for specialized cellular tasks, but direct evidence for this is limited. Transmission of noxious thermal stimuli relies on the activity of N-type $Ca_V2.2$ calcium channels in nociceptors. Using an exon-replacement strategy in mice, we show that mutually exclusive splicing patterns in the $Ca_V2.2$ gene modulate N-type channel function in nociceptors, leading to a change in morphine analgesia. Exon 37a (e37a) enhances μ-opioid receptor–mediated inhibition of N-type calcium channels by promoting activity-independent inhibition. In the absence of e37a, spinal morphine analgesia is weakened *in vivo* but the basal response to noxious thermal stimuli is not altered. Our data suggest that highly specialized, discrete cellular responsiveness *in vivo* can be attributed to alternative splicing events regulated at the level of individual neurons.

Alternative pre-mRNA splicing is used extensively in the nervous systems of complex organisms, including humans[1–3]. Transcriptome analyses suggest that alternative pre-mRNA splicing events occur in the vast majority of multi-exon human genes[4]. Furthermore, an increasing number of human diseases are linked to defects in alternative splicing[5]. Neurons are thought to use alternative splicing to add and subtract discrete protein modules encoded by alternative exons, optimizing protein function for specific cellular tasks. There is evidence that cell-dependent inclusions of alternatively spliced exons in ion channels and receptors act like molecular switches, permitting new interactions that control channel gating and receptor targeting[1,6,7]. However, there are few studies linking a specific splicing event in an identified population of neurons to changes in native protein function and behavior[1,2]. The challenge is perhaps greatest in the nervous system, where a heterogeneous population of neurons express a vast number of multi-exon genes[2,8]. Here we study the function of one site of alternative splicing in the *Cacna1b* gene, which encodes the pore-forming subunit of the N-type channel.

Ion channels underlie all electrical signals in the nervous system[9]. They are highly sensitive to perturbations in their structure or chemical environment. Moreover, these changes can be monitored with precision. Studies of ion-channel splice isoforms have shown that alternatively spliced exons in ion channels can modify plasma membrane and subcellular targeting and trafficking, second-messenger sensitivities and channel gating properties[1,6,10].

Alternatively spliced exons in genes encoding voltage-gated calcium channels have been shown to have tissue-specific expression patterns and to modify channel activity and drug sensitivity[1,7,11–15]. But there is little data on the cellular consequences in neurons and none on the behavioral consequences of regulated alternative splicing events. We have focused on *Cacna1b*, the gene encoding the presynaptic calcium channel $Ca_V2.2$, which is the core of the N-type calcium channel. In particular, we focus on a pair of mutually exclusive exons in $Ca_V2.2$ mRNA, e37a and e37b, which encode 32 amino acid residues in the proximal region of the protein's C terminus. Fourteen of the 32 residues differ between e37a and e37b. E37a has an intriguing expression profile: $Ca_V2.2$[e37a] mRNAs are enriched in nociceptors of dorsal root ganglia (DRG) and expressed at lower levels in other regions, including brain, while $Ca_V2.2$[e37b] mRNAs are ubiquitous in the nervous system[16,17]. By studying clones of $Ca_V2.2$ splice isoforms expressed in a mammalian cell line, we have previously shown that e37a creates an inhibitory domain in the $Ca_V2.2$ protein that renders N-type calcium channels sensitive to a form of $G_{i/o}$ protein–dependent inhibition that persists when cells are depolarized[7]. We have also found that e37a promotes greater N-type current density[16,17]. *In vivo* silencing of $Ca_V2.2$[e37a] reduces basal thermal nociception, suggesting this isoform participates in transmission at C-fiber terminals[18]. But the role of $Ca_V2.2$[e37a] channels in $G_{i/o}$ protein inhibition of native N-type channels in the pain pathway remains unexplored.

With this in mind, we devised a mouse model to determine why $Ca_V2.2$[e37a] channels are enriched in nociceptors of DRG. We eliminated e37a from the mouse *Cacna1b* gene and replaced it with a second 37b-encoding exon. By comparing these mice to wild-type mice that express both e37a and e37b isoforms, we show that e37a regulates μ-opioid receptor–mediated inhibition of native N-type calcium channels in nociceptors and that spinal-level analgesia by morphine *in vivo* is reduced in the absence of e37a by a mechanism that does not affect basal transmission of noxious thermal stimuli.

RESULTS

Exon substitution in the *Cacna1b* mouse gene

To determine how e37a affects N-type calcium channel activity *in vivo*, we chose an exon-substitution strategy aimed at eliminating

[1]Department of Neuroscience, Brown University, Providence, Rhode Island, USA. [2]These authors contributed equally to this work. Correspondence should be addressed to D.L. (diane_lipscombe@brown.edu).

Received 6 July; accepted 23 August; published online 19 September 2010; doi:10.1038/nn.2643

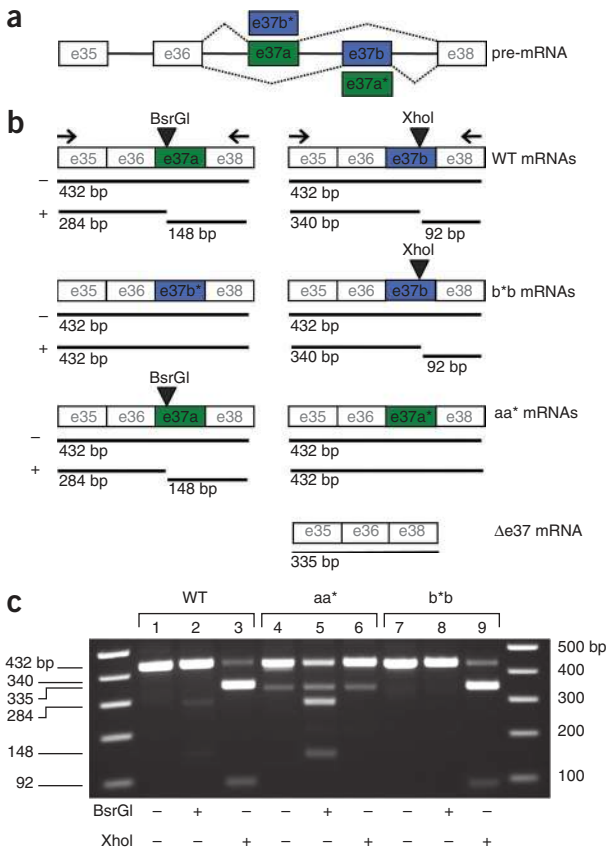

Figure 1 Exon 37 substitution in *Cacna1b* and resultant mRNAs in wild-type and mutant DRG. (**a**) Schematic of *Cacna1b* gene showing mutually exclusive exons e37a (green) and e37b (blue) with constitutively expressed exons (e35, e36 and e38). (**b**) Exon-replacement strategy and predicted mRNAs. E37b* replaces e37a, and e37a* replaces e37b to generate *Cacna1b*$^{b*b/b*b}$ (b*b) and *Cacna1b*$^{aa*/aa*}$ (aa*) mice, respectively. Shown under exon diagrams are predicted products when $Ca_V2.2$ mRNAs derived from DRG of wild-type, b*b and aa* mice are subjected to RT-PCR with primers located in exons 35 and 38. Sizes of PCR products undigested (–) and digested with BsrGI or XhoI (+) are indicated. Uncut cDNAs containing either e37a or e37b are 432 bp, and cDNAs lacking either e37a or e37b (Δ37) are 335 bp. BsrGI cuts wild-type e37a into 284-bp and 148-bp products, and XhoI cuts wild-type e37b into 340-bp and 92-bp products. Mutant e37a*– and mutant e37b*–containing sequences lack BsrGI and XhoI sites, respectively. (**c**) Results of RT-PCR from 1 μg of total RNA isolated from mouse DRG of wild-type (lanes 1–3), aa* (lanes 4–6) and b*b (lanes 7–9) mice. PCR products untreated (lanes 1, 4 and 7) and treated with BsrGI (lanes 2, 5 and 8) or XhoI (lanes 3, 6 and 9) were separated on a 2% TAE agarose gel. Lanes 1–9 are flanked by 1 kb Plus DNA ladders. A 335-bp product was amplified from DRG of aa* mice and was resistant to BsrGI and XhoI. Sequencing showed that it corresponds to mRNA lacking e37 (Δ37).

the $Ca_V2.2$[e37a] splice isoform while preserving cell-directed splicing and N-type channel expression. **Figure 1** illustrates our approach. E37a and e37b are mutually exclusive and identical in size, and can substitute for each other structurally and, in part, functionally. We replaced e37a in the mouse *Cacna1b* gene with an e37b sequence (e37b*), creating tandem 37b exons (*Cacna1b*$^{b*b/b*b}$) and eliminating e37a; we also generated mice expressing e37a only (*Cacna1b*$^{aa*/aa*}$) by the same strategy, replacing e37b in *Cacna1b* with e37a sequence (e37a*) (**Fig. 1** and **Supplementary Fig. 1**). Correct *Cacna1b* targeting was verified by genomic PCR (**Supplementary Fig. 1**) and sequencing. Mice homozygous for each mutation, *Cacna1b*$^{b*b/b*b}$ and *Cacna1b*$^{aa*/aa*}$, were viable and fecund. *Cacna1b*$^{b*b/b*b}$ homozygotes were born at wild-type frequencies, but *Cacna1b*$^{aa*/aa*}$ homozygotes were born at ~50% of the expected Mendelian rate (**Supplementary Table 1**). Our data suggest that *Cacna1b*$^{b*b/b*b}$ homozygotes tolerate e37b* as a replacement exon for e37a, whereas *Cacna1b*$^{aa*/aa*}$ homozygotes are physiologically compromised. These results point to a global disruption of N-type calcium channel function (**Supplementary Table 1**).

To distinguish mutant (e37a* and e37b*) from wild-type expressed sequences (e37a and e37b) we introduced synonymous point mutations. We eliminated the BsrGI restriction site in e37a and the XhoI restriction site in e37b. A combination of reverse-transcription PCR (RT-PCR) and restriction digest analysis showed that e37b*- and e37a*-containing mRNAs were expressed in DRG of mutant mice (**Fig. 1b**,**c** and **Supplementary Fig. 1**).

Alternative splicing patterns were comparable for *Cacna1b*$^{b*b/b*b}$ and wild-type mice in DRG. Although not quantitative, our PCR analyses suggest that the proportion of e37b* in mutants was similar to that of e37a in wild-type DRG (**Fig. 1c**). Similarly, the proportion of e37b-derived RT-PCR products amplified in mutants was comparable to that of e37b-derived products in wild-type DRG (**Fig. 1c**). These results, combined with our previous studies in rat, suggest that e37a-containing mRNAs are enriched in DRG relative to other parts of the nervous system but $Ca_V2.2$[e37b] mRNAs still represent the most common $Ca_V2.2$ isoform in RNA of whole DRG[16,17].

In contrast, expression patterns of $Ca_V2.2$[e37a] and $Ca_V2.2$[e37a*] mRNAs in DRG of *Cacna1b*$^{aa*/aa*}$ mice are different from those in wild-type mice (**Fig. 1c**). First, from *Cacna1b*$^{aa*/aa*}$ DRG we amplified a PCR product of 335 base pairs (bp) that was resistant to both XhoI and BsrGI cleavage (**Fig. 1c**). DNA sequence analysis showed this cDNA product was amplified from $Ca_V2.2$ mRNAs that lacked exon 37 (Δ37; **Fig. 1b**). We know from our previous analyses that $Ca_V2.2$ mRNAs lacking both e37a and e37b create a shift in the reading frame, an early stop codon, and nonfunctional $Ca_V2.2$ protein[19]. Second, the relative abundances of e37a- and e37a*-containing $Ca_V2.2$ mRNAs in DRG of *Cacna1b*$^{aa*/aa*}$ mice are different from those of $Ca_V2.2$[e37a] and $Ca_V2.2$[e37b] mRNAs in wild-type mice (**Fig. 1c**). Below we show that N-type currents and $Ca_V2.2$ protein levels in DRG of *Cacna1b*$^{aa*/aa*}$ mice are also substantially reduced relative to wild-type mice.

Ca^{2+} currents in DRG of *Cacna1b*$^{b*b/b*b}$ and wild-type mice

We have previously reported that $Ca_V2.2$[e37a] mRNAs are enriched in DRG, specifically in small-diameter nociceptors defined by their capsaicin sensitivity[16]. We have also shown in a mammalian expression system that e37a promotes voltage-independent inhibition of N-type currents through μ-opioid receptor activation[7]. To test the role of e37a in mediating inhibition of native N-type current in capsaicin-responsive small-diameter neurons of DRG, we first distinguished these neurons from two other classes of neurons (large and T-rich). We did this by assessing capsaicin sensitivity, cell capacitance (size) and calcium channel properties (**Supplementary Fig. 2**).

Small neurons had small membrane capacitances tightly distributed around an average value of 13 pF. These were readily separable from large neurons (37 pF; **Supplementary Fig. 2**). We found the vast majority of small neurons were capsaicin responsive (17 of 21; **Supplementary Fig. 2**), whereas large neurons rarely responded to capsaicin (1 of 19; **Supplementary Fig. 2**). A third group of neurons (T-rich[20]) expressed large T-type calcium currents that characteristically activate at low voltages and deactivate with slow kinetics (**Fig. 2**).

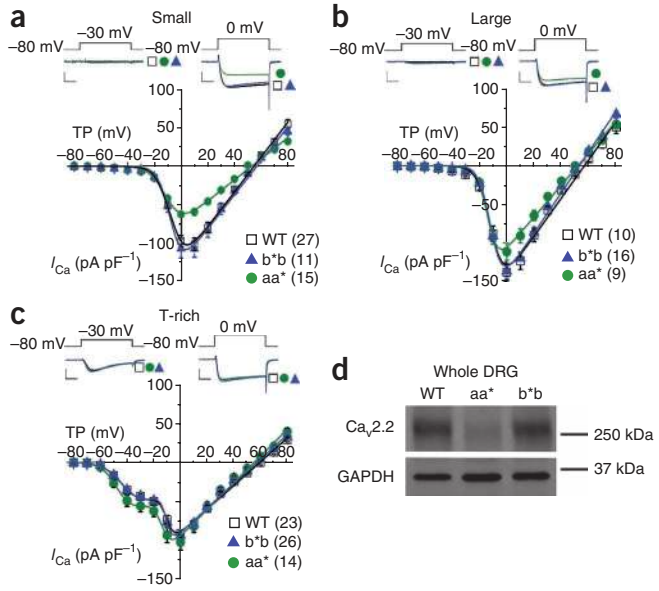

Figure 2 Whole-cell calcium current densities in DRG neurons of *Cacna1b*$^{b*b/b*b}$ mice are indistinguishable from wild-type DRG neurons. (**a**–**c**) Average current-voltage relationships in three types of DRG neurons from wild-type, *Cacna1b*$^{b*b/b*b}$ (b*b) and *Cacna1b*$^{aa*/aa*}$ (aa*) mice. Currents were evoked by test pulses to –30 mV (left) and 0 mV (right) from a holding potential of –80 mV. A series of currents were elicited by depolarizations applied every 10 s to test potentials between –70 mV and +80 mV from a holding potential of –80 mV. Current densities are plotted (pA/pF) for small cells (**a**, 13pF), large cells (**b**, 35pF) and T-rich cells (**c**, 24pF). Calcium current densities of small (**a**) and large (**b**) neurons from *Cacna1b*$^{aa*/aa*}$ mice were significantly smaller than those from wild-type mice ($P = 0.0004$ and $P = 0.03$, respectively). Individual current voltage plots were fit with one (**a**,**b**) or two (**c**) Boltzmann functions using average parameters calculated from fitting individual curves (**Supplementary Table 2**). Scale bars, 500 pA and 5 ms. Data are means ± s.e.m. *n* values shown in parentheses are number of cells; all data sets contain recordings from at least nine mice. (**d**) Western blot of DRG lysates derived from wild-type, aa* and b*b mice using a polyclonal antibody directed to $Ca_V2.2$ and a monoclonal antibody directed to glyceraldehyde 3-phosphate dehydrogenase (GAPDH). $Ca_V2.2$ protein levels in DRG of aa* mice were lower than in wild-type mice. $Ca_V2.2$ protein runs at 260 kDa; location of a 250-kDa size marker is indicated. Complete, uncropped blots are shown in **Supplementary Figure 5**.

These were intermediate in size and did not respond to capsaicin, but by virtue of their large T-type currents they were easily identified and separated from small and large neurons (**Supplementary Fig. 2**).

Whole-cell calcium currents in all three groups of DRG neurons from *Cacna1b*$^{b*b/b*b}$ mice were indistinguishable from those in wild type mice (*Cacna1b*$^{ab/ab}$; **Fig. 2a–c**). DRG neurons express at least four different classes of calcium channels, N-type, P/Q-type, L-type and T-type; N-type represents the largest component[16,20,21]. We isolated pure N-type from non–N-type currents using the N-type calcium channel blocker 2 μM ω-conotoxin GVIA and found that N-type currents in DRG neurons of *Cacna1b*$^{b*b/b*b}$ mice were also indistinguishable from the wild type (**Fig. 3**). These data support our RT-PCR analyses that show e37b* can substitute for e37a and support wild-type splicing patterns in DRG neurons.

N-type Ca^{2+} currents in aa* mice are smaller than in wild type

In contrast to *Cacna1b*$^{b*b/b*b}$, N-type currents in small and large neurons of *Cacna1b*$^{aa*/aa*}$ mice were significantly smaller than in wild-type mice (Student's *t*-test, $P = 0.000238$; **Fig. 3a**). In addition, T-type currents in T-rich neurons were slightly larger than in wild-type mice, but the difference was not statistically significant (Student's *t*-test, $P = 0.245$; **Figs. 2** and **3**). $Ca_V2.2$ protein levels in DRG (**Fig. 2d**) and in brains (**Supplementary Fig. 3**) of *Cacna1b*$^{aa*/aa*}$ mice were reduced relative to wild-type mice. This reduction was specific to $Ca_V2.2$ protein and did not lead to compensatory changes in levels of the closely related $Ca_V2.1$ protein in brains of *Cacna1b*$^{aa*/aa*}$ mice. The reduction in $Ca_V2.2$ protein levels in DRG of *Cacna1b*$^{aa*/aa*}$ mice could not be explained by differences in cell size; whole-cell capacitance values within

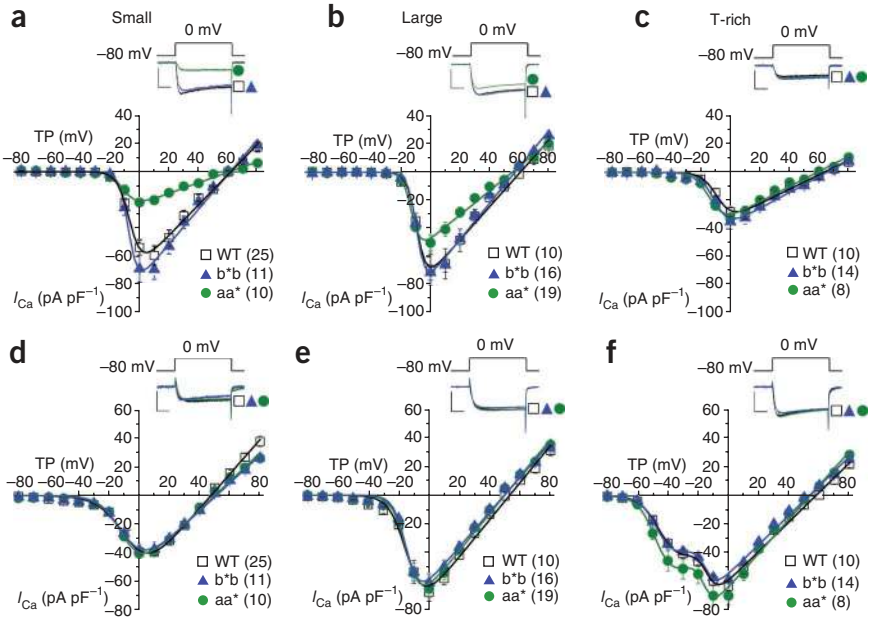

Figure 3 N-type and non–N-type current densities in sensory neurons of *Cacna1b*$^{b*b/b*b}$ mice are indistinguishable from those in wild-type mice. (**a**–**f**) Average N-type (**a**–**c**) and non–N-type (**d**–**f**) calcium current–voltage relationships in three subtypes (small, large and T-rich) of acutely dissociated DRG neurons from wild-type, *Cacna1b*$^{b*b/b*b}$ (b*b) and *Cacna1b*$^{aa*/aa*}$ (aa*) mice. Representative currents shown above current voltage plots were evoked by test pulses to 0 mV from a holding potential of –80 mV and were recorded from each cell type and each mouse line. Currents were elicited as described in **Figure 2** and plotted as pA/pF to normalize for cell size. N-type currents and non–N-type currents correspond to ω-conotoxin GVIA–sensitive and ω-conotoxin GVIA–insensitive components of the whole-cell current, respectively. We isolated N-type currents in each cell by subtracting non–N-type currents (insensitive to 2 μM ω-conotoxin GVIA) from whole-cell currents. N-type current densities in small (**a**) and large (**b**) neurons were significantly smaller in *Cacna1b*$^{aa*/aa*}$ mice than in wild-type mice ($P = 0.0003$ and $P = 0.0038$, respectively). Individual current voltage plots were fit with one (**a**–**e**) or two (**f**) Boltzmann functions using average parameters calculated from fitting individual curves (**Supplementary Table 2**). Scale bars, 500 pA and 5 ms. Data are means ± s.e.m. *n* values in parentheses are number of cells; all data sets contain recordings from at least nine mice.

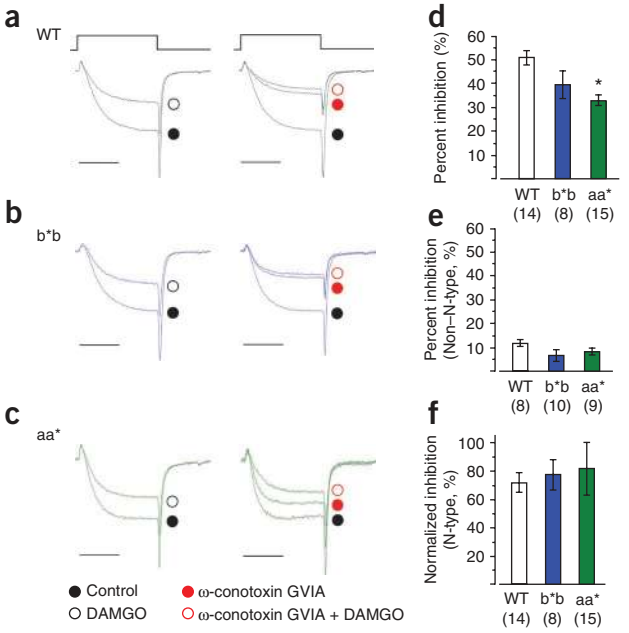

Figure 4 DAMGO inhibits N-type currents similarly in nociceptors from all three genotypes. (**a**–**c**) Representative currents from nociceptors isolated from wild-type (**a**), *Cacna1b*$^{b*b/b*b}$ (b*b; **b**) and *Cacna1b*$^{aa*/aa*}$ (aa*; **c**) mice show the inhibitory actions of a saturating concentration of 10 μM DAMGO on calcium currents in the absence (left; whole-cell currents) or presence (right; non–N-type currents) of ω-conotoxin GVIA (2 μM). For comparison, current amplitudes are scaled relative to their respective controls. Currents were elicited by test pulses to 0 mV from a holding potential of –80 mV. Scale bar, 5 ms. (**d**,**e**) Average percent inhibition by DAMGO in nociceptors of wild-type, b*b, and aa* mice in the absence (**d**; whole-cell current) or presence (**e**; non–N-type current) of 2 μM ω-conotoxin GVIA. Values shown are means ± s.e.m. *n* values in parentheses are number of cells; all data sets contain recordings from at least nine mice. DAMGO was significantly less effective at inhibiting whole-cell currents in aa* mice than in wild-type mice (**d**; $P = 0.0432$). (**f**) DAMGO's inhibition of N-type currents in nociceptors, compared among the three genotypes. For comparison, because N-type current density was substantially smaller in nociceptors of aa* mice, percent inhibition by DAMGO was normalized to N-type current density with the following formula: $100\% \times ((I_{control} - I_{DAMGO}) - (I_{\omega\text{-conotoxin}} - I_{DAMGO}))/I_{N\text{-type}}$. $I_{control} - I_{DAMGO}$ represents whole-cell current; $I_{\omega\text{-conotoxin}} - I_{DAMGO}$ represents non–N-type current. Average values of $I_{\omega\text{-conotoxin}}$, I_{DAMGO} and $I_{N\text{-type}}$ were obtained from nociceptors of wild-type ($n = 8$), b*b ($n = 10$) and aa* ($n = 9$) mice for these calculations.

each subset of neurons were indistinguishable among genotypes (**Supplementary Fig. 2**). Furthermore, we compared calcium current densities (pA pF^{-1}) to normalize for cell size (**Figs. 2** and **3**). N-type currents in all three groups of DRG neurons from *Cacna1b*$^{aa*/aa*}$ mice activated at voltages ~7 mV more hyperpolarized than the voltages at which N-type currents were activated in neurons of wild-type and *Cacna1b*$^{b*b/b*b}$ mice (**Fig. 3a**–**c**). Our findings are highly consistent with our previous studies of cloned e37a-containing N-type channels expressed in mammalian and amphibian cells. These similarly activated at voltages ~7 mV more hyperpolarized than e37b-containing N-type channels[7,16,17].

The reduction of $Ca_V2.2$ protein levels in *Cacna1b*$^{aa*/aa*}$ mice probably results from a disruption in alternative splicing, consistent with the data from e37a-lacking $Ca_V2.2$ mRNAs in DRG (**Fig. 1c**). We next compared G protein inhibition of N-type currents in small-diameter nociceptors from our various mouse lines, but with our primary focus on *Cacna1b*$^{b*b/b*b}$ and wild-type recordings, because $Ca_V2.2$ protein levels are reduced in *Cacna1b*$^{aa*/aa*}$ mice.

DAMGO inhibits Ca^{2+} currents in all genotypes similarly

In previous studies of cloned $Ca_V2.2$[e37a] and $Ca_V2.2$[e37b] channels in a mammalian cell line, we have shown that e37a-containing N-type channels promote voltage-independent inhibition of N-type currents via G protein–coupled receptors without affecting overall inhibition of peak current[7]. We next tested whether e37a regulates the responsiveness of native N-type currents to μ-opioid receptor–mediated inhibition in nociceptors that express both $Ca_V2.2$[e37a] and $Ca_V2.2$[e37b] mRNAs under normal circumstances[16].

We used a saturating concentration of the opioid peptide DAMGO (10 μM) to activate μ-opioid receptors and monitored the effects on N-type and non–N-type currents in nociceptors of *Cacna1b*$^{b*b/b*b}$ and wild-type mice (**Fig. 4**). Overall, we found DAMGO was a more effective inhibitor of N-type (70–75%) than of non–N-type (15–25%) current, as reported elsewhere[21]. DAMGO inhibited N-type current amplitudes in nociceptors from *Cacna1b*$^{b*b/b*b}$ and wild-type mice equally ($P = 0.64$; **Fig. 4f**). Similarly, the efficacy of DAMGO on N-type currents in small neurons of *Cacna1b*$^{aa*/aa*}$ mice was not significantly different from its efficacy in wild-type mice ($P = 0.49$; **Fig. 4f**).

E37a promotes voltage-independent inhibition by DAMGO

If e37a does not influence the overall inhibitory action of DAMGO, does it affect the type of inhibition? To answer this question, we next tested whether e37a was important for voltage-independent inhibition of N-type currents by DAMGO.

We used standard strong, brief, suprathreshold depolarizations to 80 mV just before the test pulse to remove voltage-dependent inhibition mediated by saturating concentrations of DAMGO (**Fig. 5**). This allowed us to calculate the relative amounts of voltage-dependent and voltage-independent inhibition of non–N-type and N-type currents (**Fig. 5g**,**h**). DAMGO inhibited non–N-type currents by voltage-dependent and voltage-independent mechanisms, and the relative contribution of each was the same in neurons of wild-type, *Cacna1b*$^{b*b/b*b}$ and *Cacna1b*$^{aa*/aa*}$ mice (70% voltage-independent; **Fig. 5d**–**f**,**h**).

However, we observed substantial differences when we compared DAMGO's effects on N-type currents in nociceptors of *Cacna1b*$^{b*b/b*b}$ mice compared with wild-type mice ($P = 0.032$; **Fig. 5g**). Even though peak N-type currents in nociceptors of all three genotypes were inhibited equally well by DAMGO (**Fig. 4**), its inhibitory effects were mostly voltage-dependent in neurons of *Cacna1b*$^{b*b/b*b}$ mice (75% voltage-dependent; **Fig. 5b**,**g**), in contrast to wild-type mice (50% voltage-dependent; **Fig. 5a**,**g**). In other words, DAMGO caused significantly less voltage-independent inhibition of N-type currents in nociceptors of *Cacna1b*$^{b*b/b*b}$ mice. It was only in nociceptors of *Cacna1b*$^{b*b/b*b}$ mice that we observed a shift from voltage-independent toward voltage-dependent inhibition of N-type currents; DAMGO's effects on N-type currents in nociceptors of *Cacna1b*$^{aa*/aa*}$ mice (**Fig. 5c**,**g**) and on non–N-type currents in *Cacna1b*$^{b*b/b*b}$ and *Cacna1b*$^{aa*/aa*}$ mice (**Fig. 5e**,**f**,**h**) were the same as in wild-type mice. This is generally consistent with our studies of cloned $Ca_V2.2$[e37a] and $Ca_V2.2$[e37b] channels expressed in tsA201 cells[7].

E37a influences spinal-level analgesia by morphine

Our electrophysiological analyses show that e37a promotes a form of N-type channel inhibition in nociceptors that is resistant to depolarization (voltage-independent). We also compared the overall distribution of $Ca_V2.2$ protein in the dorsal spinal horn of wild-type, *Cacna1b*$^{b*b/b*b}$ and *Cacna1b*$^{aa*/aa*}$ mice by immunohistochemistry.

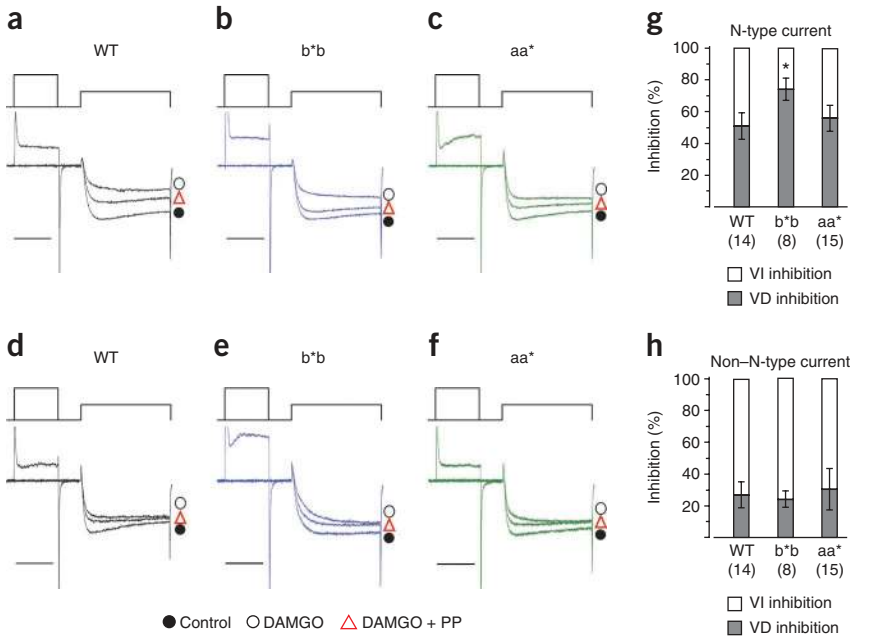

Figure 5 Voltage-independent inhibition by DAMGO is reduced in nociceptors that only express e37b and not e37a. (**a**–**f**) Representative currents from small neurons isolated from wild-type (**a**,**d**), *Cacna1b*$^{b*b/b*b}$ (b*b; **b**,**e**) and aa* (**c**,**f**) mice show the inhibitory actions of 10 μM DAMGO on whole-cell currents in the absence (**a**–**c**; whole-cell currents) or presence (**d**–**f**) of ω-conotoxin GVIA (2 μM). Currents were elicited by test pulses to 0 mV from a holding potential of –80 mV without or with a strong prepulse (+ PP) to +80 mV to remove voltage-dependent inhibition. For comparison, current amplitudes are scaled relative to their respective controls. Scale bar, 5 ms. (**g**,**h**) Relative amount of voltage-dependent and voltage-independent inhibition of N-type (**g**; $P = 0.0321$) and non–N-type (**h**) currents mediated by 10 μM DAMGO in recordings from nociceptors of wild-type, b*b and aa* mice. VI, voltage-independent component of inhibition; VD, voltage-dependent component. Values shown are means ± s.e.m. *n* values shown are number of cells; all data sets contain recordings from at least nine mouse lines. Percent voltage-independent inhibition of N-type current was estimated as follows: $100\% \times (VI_{whole\text{-}cell} - VI_{non\text{–}N\text{-}type})$/total N-type inhibition.

The overall pattern of anti-$Ca_V2.2$ signal was similar among the three genotypes, as were gross patterns of anti-CGRP signal and IB4 fluorescence. Although not quantitative, these signals suggest there are no gross disruptions of $Ca_V2.2$ distribution in afferent terminals in the superficial laminae of the dorsal spinal horn where afferents of nociceptors terminate (**Fig. 6**).

We next used our mouse models to test the role of e37a in (i) basal nociception and (ii) spinal analgesia by morphine. Small capsaicin-responsive nociceptors transmit information about noxious thermal stimuli. Intrathecal morphine, acting through μ-opioid receptors, inhibits transmission in this pathway[22,23]. At least part of morphine's spinal-level analgesia is through μ-opioid receptor–mediated inhibition of presynaptic N-type channels on nociceptor terminals in the dorsal horn of the spinal cord[24,25]. To assess this pathway, we applied standard thermal stimuli to the hind paw and measured paw-withdrawal latencies in all three mouse lines. This behavioral test specifically assesses spinal-level circuits[26,27]. Paw-withdrawal latencies measured from wild-type, *Cacna1b*$^{b*b/b*b}$ and *Cacna1b*$^{aa*/aa*}$ mice were the same (**Fig. 7a**). Our data suggest that amino acid residues unique to e37a are not necessary for normal transmission of noxious thermal stimuli.

Finally, we tested whether e37a contributes to the analgesic actions of intrathecal morphine. This route of administration restricts the site of morphine action to the spinal cord and rules out contributions from supraspinal sites[28,29]. At doses higher than 3 μg, morphine induced behavior that interfered with testing. At its peak, 3 μg morphine induced analgesia to a level 70% of the maximum possible effect against the thermal stimulus, similar to other reported results[30]. We found substantial differences in the analgesic efficacy of intrathecal morphine in *Cacna1b*$^{b*b/b*b}$ mice compared with wild-type mice

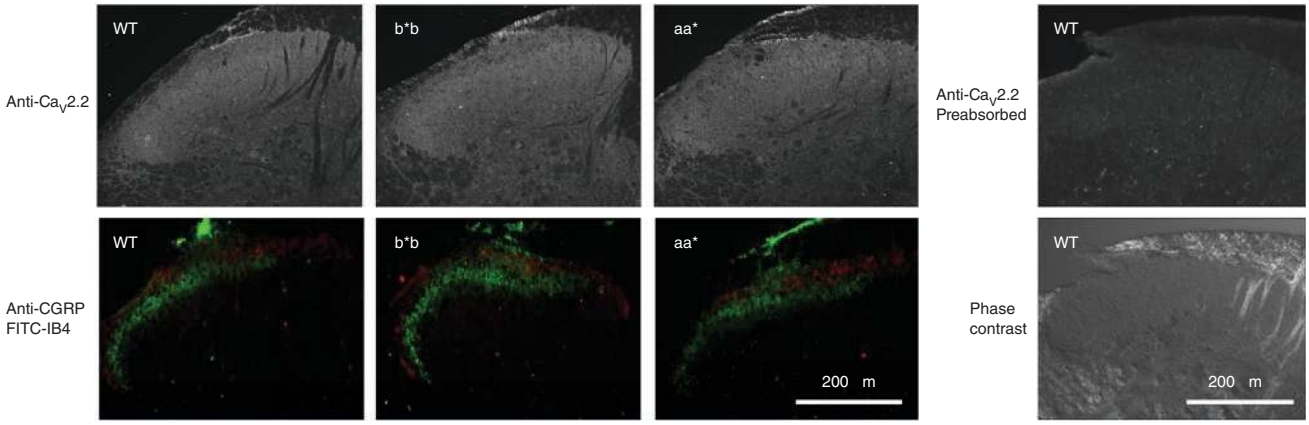

Figure 6 Anti-$Ca_V2.2$, anti-CGRP and FITC-IB4 signals in superficial layers of dorsal spinal horn are similar among genotypes. Spinal cord sections from wild-type, *Cacna1b*$^{b*b/b*b}$ (b*b) and *Cacna1b*$^{aa*/aa*}$ (aa*) mice show the dorsal spinal horn. The anti-$Ca_V2.2$ immunofluorescence signal is similar among the three genotypes (upper images), as are the anti-CGRP (red, lower images) and FITC-IB4 (green, lower images) signals. Lower images show prominent CGRP and IB4 fluorescence in laminae I and II of the dorsal horn. CGRP and IB4 are often used to mark peptidergic and non-peptidergic nociceptive terminals, respectively[49,50]. A spinal cord section from wild-type mice incubated with the primary antibody preabsorbed with the corresponding antigenic peptide is shown as control. Phase-contrast image of the same section is also shown. The antigenic peptide control shows complete loss of $Ca_V2.2$ staining. The anti-$Ca_V2.2$ signal is seen throughout the dorsal spinal horn, but there is an enhanced signal in the superficial laminae in the region of the IB4 and CGRP signals.

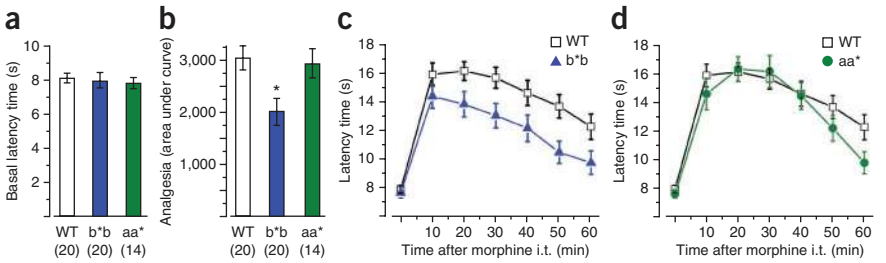

Figure 7 Morphine's spinal-level analgesia is reduced in mice that lack e37a. (**a**,**b**) Comparison of thermal pain thresholds in wild-type ($n = 20$), *Cacna1b*$^{b*b/b*b}$ (b*b; $n = 20$) and *Cacna1b*$^{aa*/aa*}$ (aa*; $n = 14$) mice before (**a**) and after (**b**) intrathecal morphine. Average basal paw-withdrawal latencies (PWLs; Hargreaves's test) in response to noxious thermal stimuli were not significantly different in wild-type, b*b and aa* mice (**a**; Student's *t*-test, $P > 0.5$). In **b**, to normalize for differences in baseline responsiveness among mice, intrathecal morphine analgesia was expressed as the integral (area under the curve) of the percentage of maximum possible effect (%MPE) for each group, where $\%MPE = (PWL_{morphine} - PWL_{baseline})100/(20 - PWL_{baseline})$. Morphine was significantly less effective against thermal stimuli in b*b mice than in wild-type mice (Student's *t*-test, $P = 0.004$) but had similar efficacy in aa* and wild-type mice (Student's *t*-test, $P = 0.77$). (**c**,**d**) Time course of morphine analgesia after intrathecal (i.t.) injection (3 μg) at time 0 in wild-type and b*b mice (**c**) and in wild-type and aa* mice (**d**). The efficacy of morphine is reduced in b*b mice relative to wild-type mice. *P* values at 0, 10, 20, 30, 40, 50 and 60 min were 0.613, 0.190, 0.043, 0.023, 0.061, 0.008 and 0.044, respectively, comparing average responses in b*b and wild-type mice (Student's two-tailed *t*-test; **c**). Values shown are means ± s.e.m.

(**Fig. 7b–d**). As reported[29], intrathecal morphine transiently lengthened latencies of paw withdrawal in response to thermal stimuli. Overall, morphine was 30% less effective as an analgesic at 3 μg in *Cacna1b*$^{b*b/b*b}$ than in wild-type mice ($n = 20$, Student's two-tailed *t*-test, $P = 0.004$; **Fig. 7b**). By comparison, morphine was similarly effective at prolonging paw-withdrawal latencies in *Cacna1b*$^{aa*/aa*}$ and wild-type mice ($n = 14$, $P = 0.77$; **Fig. 7b**). We compared the time courses of morphine-induced analgesia in *Cacna1b*$^{b*b/b*b}$, *Cacna1b*$^{aa*/aa*}$ and wild-type mice (**Fig. 7c**,**d**). The analgesic effect of 3 μg morphine was apparent within 10 min and peaked at 20–30 min; the effect was reduced in *Cacna1b*$^{b*b/b*b}$ mice at all time points tested. These differences are significant at 20, 30, 50 and 60 min (Student's two-tailed *t*-test, $P = 0.008–0.044$; **Fig. 7c**).

Finally, we compared the efficacy of two lower doses of intrathecal morphine in wild-type and *Cacna1b*$^{b*b/b*b}$ mice. Although there is no significant difference between wild-type and *Cacna1b*$^{b*b/b*b}$ mice in the overall efficacy of morphine at 0.1 μg and 0.3 μg ($P = 0.69$ and $P = 0.75$, respectively; **Supplementary Fig. 4**), the dose-response relationships are significantly different, as indicated by their slopes (Student's *t*-test, $P = 0.04$; **Supplementary Fig. 4**). Our data suggest that e37a is needed for the maximal spinal-level analgesic actions of morphine at higher doses, in response to noxious thermal stimuli.

DISCUSSION

Cell-directed alternative pre-mRNA splicing is thought to represent an important step in optimizing protein function for specialized tasks, but few if any studies have linked a single splicing event to a specific behavior in mammals[1,2]. We used an exon-replacement strategy to show that it is possible to attribute a decrease in the efficacy of morphine to a single RNA processing event. We suggest that cell-specific selection of e37a during alternative pre-mRNA splicing enhances activity-independent G protein inhibition of N-type calcium channels in nociceptors. The enrichment of e37a in nociceptors may augment the analgesic actions of morphine *in vivo*.

Intrathecal morphine may need e37a for maximal efficacy

Our approach took advantage of a localized splicing event in a well-described population of functionally specialized neurons, which underlie a behavior that can be measured reliably. Capsaicin-responsive small-diameter nociceptors of unmyelinated C-fibers are specialized to transmit noxious thermal stimuli[22,31]. N-type $Ca_V2.2$ calcium channels at presynaptic terminals of C-fiber afferents in the spinal cord mediate transmitter release and behavioral responses to noxious stimuli[32]. Morphine occludes transmission of noxious thermal stimuli in the spinal cord in large part by μ-opioid receptor–mediated inhibition of presynaptic N-type channels at nociceptor terminals[32–36]. By comparing behavioral responses in *Cacna1b*$^{b*b/b*b}$ and wild-type mice, we have obtained evidence that maximal analgesic actions of intrathecal morphine may depend on e37a-containing $Ca_V2.2$ channels (**Fig. 7**). Collectively, our studies support the hypothesis that e37a boosts the analgesic effects of morphine via its influence on μ-opioid receptor–mediated inhibition of N-type calcium channels. E37a selectively augments voltage-independent inhibition of N-type currents without affecting the overall level of current inhibition (**Figs. 4**, **5** and **7**). Our conclusions about the role of e37a from the present studies on native channels and receptors are reinforced by our previous studies of cloned $Ca_V2.2$ isoforms and receptors expressed in the tsA201 cell line[7].

Our analyses of *Cacna1b*$^{b*b/b*b}$ and wild-type mice suggest that, at higher doses, about 30% of morphine's analgesic actions at the level of the spinal cord rely on e37a-dependent inhibition of N-type channels. E37a-independent actions of morphine probably include voltage-dependent and voltage-independent inhibition of N-type calcium channels, and postsynaptic GIRK potassium channel activation via μ-opioid receptors[30]. Notably, the GIRK-dependent component of spinal analgesia by morphine is similar in magnitude and is engaged at the same concentration of morphine as we report for e37a[30].

Paw-withdrawal latencies to noxious thermal stimuli were indistinguishable among genotypes, suggesting that $Ca_V2.2$[e37a] and $Ca_V2.2$[e37b] channels support transmission of nociceptive information in the spinal cord equally well. By contrast, studies using isoform-specific small interfering RNA suggest that $Ca_V2.2$[e37a] channels have a preferred role in transmission of noxious thermal stimuli[18], in apparent contradiction to our analyses of *Cacna1b*$^{b*b/b*b}$ mice. However, these two observations might be reconcilable if $Ca_V2.2$[e37a] channels localize preferentially at transmitter release sites in nerve terminals of nociceptors of wild-type mice and in their absence (*Cacna1b*$^{b*b/b*b}$), $Ca_V2.2$[e37b] channels target to these presynaptic locations and support transmission of nociception with similar efficacy. There are no gross differences in anti-$Ca_V2.2$ signals in dorsal spinal horn among genotypes (**Supplementary Fig. 4**), but experiments designed to quantify the density of presynaptic N-type channels would be needed to test these and other possibilities.

Cacna1b$^{aa*/aa*}$ mice are physiologically compromised, but our behavioral analyses suggest that transmission of nociceptive signals and morphine's analgesic actions are very similar to those in wild-type mice. This might be unexpected, because N-type currents

and $Ca_V2.2$ protein levels are reduced in DRG neurons, but the results are consistent with reports that withdrawal latencies to thermal stimuli are unchanged in *Cacna1b*$^{-/-}$ null mice compared with wild-type mice[33,37]. As noted above, experiments are needed to measure the relative contribution of N-type currents to transmission in the dorsal spinal horn.

Voltage-independent inhibition and morphine analgesia

Voltage-independent inhibition of N-type calcium currents has been studied for more than a decade[38–43]. From these and other findings, a hypothesis has developed that voltage-independent inhibition of presynaptic N-type calcium channels via G protein–coupled receptors represents a mechanism for transmitter- and drug-mediated inhibition of synaptic transmission independent of neuronal activity[33,40,41,43,44]. By contrast, a purely voltage-dependent mechanism would inhibit N-type channels and synaptic transmission most strongly during periods of low neuronal activity, but would become less effective as activity increased[40,44,45]. Voltage-independent inhibition of N-type calcium channels through $G_{i/o}$ coupled receptors and e37a might underlie some of the analgesic actions of morphine, particularly at higher doses. However, e37a may also influence other properties of N-type channels, including cellular distribution and, as we report here, N-type current densities. One or all of these could influence the spinal-level actions of morphine.

Although morphine is a highly effective analgesic in response to noxious thermal stimuli in naïve mice and humans, it is much less effective against the thermal hyperalgesia characteristic of neuropathic pain[31]. Expression levels of many genes are altered in the DRG of animals experiencing neuropathic pain. These changes have been implicated in the development and maintenance of chronic pain as well as in the loss of morphine efficacy[31]. $Ca_V2.2$ mRNA and protein levels are not thought to change in DRG after peripheral nerve injury, but as we have reported[18], $Ca_V2.2$[e37a] mRNAs are reduced. In light of the present study, it is possible that an injury-induced shift from e37a-containing to e37b-containing $Ca_V2.2$ channels in nociceptors, and therefore a concomitant change in inhibition of N-type calcium channels via μ-opioid receptors, might contribute to decreased spinal-level analgesia in response to morphine.

Cell-directed splicing of e37a

E37a is enriched in a subset of nociceptors in DRG[16]. What are the factors that control exon selection—an important step in the pain pathway—in these cells? Genome-wide analyses show that several proteins are involved in driving neuronal-specific alternative splicing[46,47], but there are few examples of how these factors coordinate exon selection in specific gene families within defined populations of neurons. Several neuronal splicing factors can function both as repressors and enhancers, depending on binding location with respect to the target exon, and exon selection probably depends on the relative contributions of several splicing factors working in concert[2,47,48]. The expression profile of e37a and the marked decrease in $Ca_V2.2$ protein levels in *Cacna1b*$^{aa*/aa*}$ mice suggest that most neurons may contain repressor activity that prevents e37a inclusion during splicing. However, our analysis of N-type current densities among small, T-rich and large cells of DRG from *Cacna1b*$^{aa*/aa*}$ mice suggest that e37a selection depends on additional factors with differential actions in these three classes of neuron. We studied *Cacna1b* gene sequences at and close to e37a and e37b splice junctions, but we have not identified the *cis* and *trans* factors that regulate alternative splicing at this site. We hope new data from genome-wide screens of splicing factor–RNA binding events will help define cell-specific mechanisms that orchestrate alternative splicing in Ca_V2 pre-mRNAs in specific neurons[46–48].

The e37a/e37b splice site is conserved in all mammalian *Cacna1b* genes, so activity unique to e37a must provide some evolutionary advantage. Our data suggest that at higher doses morphine engages e37a in spinal analgesia to thermal stimuli, but it is likely that endogenous transmitters use this inhibitory pathway to control nociception under certain conditions. Identifying cell-specific splicing factors that control alternative splicing of e37a could lead to new therapeutic approaches to increase the efficacy of drugs and neurotransmitters that work through G protein–coupled receptors to inhibit N-type calcium channels. Such studies could also provide insight into cell-specific, coordinated alternative splicing of several pre-mRNAs that contribute to setting the efficacy of transmission in the pain pathway.

METHODS

Methods and any associated references are available in the online version of the paper at http://www.nature.com/natureneuroscience/.

Note: Supplementary information is available on the Nature Neuroscience website.

ACKNOWLEDGMENTS

We thank J. Kysik and E. Paul in the mouse transgenic facility at Brown University, R. Burwell for advice on animal behavior, T.D. Helton for help with image analyses and C.G. Phillips and S.E. Allen for helpful comments on the manuscript. This work was supported by US National Institutes of Health grants RO1NS055251 (D.L.), F31NS066702 (S.M.) and P20RR015578 (Transgenic Facility at Brown University).

AUTHOR CONTRIBUTIONS

All authors contributed to writing this manuscript. A.A. carried out electrophysiological studies, S.D. designed targeting constructs and generated all exon-substituted mice, Y.-Q.J. performed the behavioral studies and immunohistochemistry, S.M. performed western analyses, and D.L. directed the project and oversaw all analyses.

COMPETING FINANCIAL INTERESTS

The authors declare no competing financial interests.

Published online at http://www.nature.com/natureneuroscience/.
Reprints and permissions information is available online at http://npg.nature.com/reprintsandpermissions/.

1. Lipscombe, D. Neuronal proteins custom designed by alternative splicing. *Curr. Opin. Neurobiol.* **15**, 358–363 (2005).
2. Li, Q., Lee, J.A. & Black, D.L. Neuronal regulation of alternative pre-mRNA splicing. *Nat. Rev. Neurosci.* **8**, 819–831 (2007).
3. Ule, J. & Darnell, R.B. RNA binding proteins and the regulation of neuronal synaptic plasticity. *Curr. Opin. Neurobiol.* **16**, 102–110 (2006).
4. Pan, Q., Shai, O., Lee, L.J., Frey, B.J. & Blencowe, B.J. Deep surveying of alternative splicing complexity in the human transcriptome by high-throughput sequencing. *Nat. Genet.* **40**, 1413–1415 (2008).
5. Dredge, B.K., Polydorides, A.D. & Darnell, R.B. The splice of life: alternative splicing and neurological disease. *Nat. Rev. Neurosci.* **2**, 43–50 (2001).
6. Mu, Y., Otsuka, T., Horton, A.C., Scott, D.B. & Ehlers, M.D. Activity-dependent mRNA splicing controls ER export and synaptic delivery of NMDA receptors. *Neuron* **40**, 581–594 (2003).
7. Raingo, J., Castiglioni, A.J. & Lipscombe, D. Alternative splicing controls G protein-dependent inhibition of N-type calcium channels in nociceptors. *Nat. Neurosci.* **10**, 285–292 (2007).
8. Chen, M. & Manley, J.L. Mechanisms of alternative splicing regulation: insights from molecular and genomics approaches. *Nat. Rev. Mol. Cell Biol.* **10**, 741–754 (2009).
9. Hille, B. *Ion Channels of Excitable Membranes* (Sinauer, Sunderland, Massachusetts, USA, 2001).
10. Xie, J. & Black, D.L.A. CaMK IV responsive RNA element mediates depolarization-induced alternative splicing of ion channels. *Nature* **410**, 936–939 (2001).
11. Mich, P.M. & Horne, W.A. Alternative splicing of the Ca^{2+} channel β4 subunit confers specificity for gabapentin inhibition of $Ca_V2.1$ trafficking. *Mol. Pharmacol.* **74**, 904–912 (2008).
12. Liao, P., Zhang, H.Y. & Soong, T.W. Alternative splicing of voltage-gated calcium channels: from molecular biology to disease. *Pflugers Arch.* **458**, 481–487 (2009).

13. Zhong, X., Liu, J.R., Kyle, J.W., Hanck, D.A. & Agnew, W.S. A profile of alternative RNA splicing and transcript variation of CACNA1H, a human T-channel gene candidate for idiopathic generalized epilepsies. *Hum. Mol. Genet.* **15**, 1497–1512 (2006).
14. Bourinet, E. *et al.* Splicing of α_{1A} subunit gene generates phenotypic variants of P- and Q-type calcium channels. *Nat. Neurosci.* **2**, 407–415 (1999).
15. Adams, P.J. *et al.* $Ca_V2.1$ P/Q-type calcium channel alternative splicing affects the functional impact of familial hemiplegic migraine mutations: implications for calcium channelopathies. *Channels (Austin)* **3**, 110–121 (2009).
16. Bell, T.J., Thaler, C., Castiglioni, A.J., Helton, T.D. & Lipscombe, D. Cell-specific alternative splicing increases calcium channel current density in the pain pathway. *Neuron* **41**, 127–138 (2004).
17. Castiglioni, A.J., Raingo, J. & Lipscombe, D. Alternative splicing in the C-terminus of CaV2.2 controls expression and gating of N-type calcium channels. *J. Physiol. (Lond.)* **576**, 119–134 (2006).
18. Altier, C. *et al.* Differential role of N-type calcium channel splice isoforms in pain. *J. Neurosci.* **27**, 6363–6373 (2007).
19. Pan, J.Q. & Lipscombe, D. Alternative splicing in the cytoplasmic II–III loop of the N-type Ca channel α_{1B} subunit: functional differences are β subunit-specific. *J. Neurosci.* **20**, 4769–4775 (2000).
20. Nelson, M.T., Joksovic, P.M., Perez-Reyes, E. & Todorovic, S.M. The endogenous redox agent L-cysteine induces T-type Ca^{2+} channel-dependent sensitization of a novel subpopulation of rat peripheral nociceptors. *J. Neurosci.* **25**, 8766–8775 (2005).
21. Taddese, A., Nah, S.Y. & McCleskey, E.W. Selective opioid inhibition of small nociceptive neurons. *Science* **270**, 1366–1369 (1995).
22. Scherrer, G. *et al.* Dissociation of the opioid receptor mechanisms that control mechanical and heat pain. *Cell* **137**, 1148–1159 (2009).
23. Glaum, S.R., Miller, R.J. & Hammond, D.L. Inhibitory actions of delta 1-, delta 2-, and mu-opioid receptor agonists on excitatory transmission in lamina II neurons of adult rat spinal cord. *J. Neurosci.* **14**, 4965–4971 (1994).
24. Bao, J., Li, J.J. & Perl, E.R. Differences in Ca^{2+} channels governing generation of miniature and evoked excitatory synaptic currents in spinal laminae I and II. *J. Neurosci.* **18**, 8740–8750 (1998).
25. Williams, J.T., Christie, M.J. & Manzoni, O. Cellular and synaptic adaptations mediating opioid dependence. *Physiol. Rev.* **81**, 299–343 (2001).
26. Wilson, S.G. & Mogil, J.S. Measuring pain in the (knockout) mouse: big challenges in a small mammal. *Behav. Brain Res.* **125**, 65–73 (2001).
27. Hargreaves, K., Dubner, R., Brown, F., Flores, C. & Joris, J. A new and sensitive method for measuring thermal nociception in cutaneous hyperalgesia. *Pain* **32**, 77–88 (1988).
28. Hylden, J.L. & Wilcox, G.L. Intrathecal morphine in mice: a new technique. *Eur. J. Pharmacol.* **67**, 313–316 (1980).
29. Wang, Y.X., Pettus, M., Gao, D., Phillips, C. & Scott Bowersox, S. Effects of intrathecal administration of ziconotide, a selective neuronal N-type calcium channel blocker, on mechanical allodynia and heat hyperalgesia in a rat model of postoperative pain. *Pain* **84**, 151–158 (2000).
30. Marker, C.L., Lujan, R., Loh, H.H. & Wickman, K. Spinal G-protein-gated potassium channels contribute in a dose-dependent manner to the analgesic effect of μ- and δ- but not κ-opioids. *J. Neurosci.* **25**, 3551–3559 (2005).
31. Costigan, M., Scholz, J. & Woolf, C.J. Neuropathic pain: a maladaptive response of the nervous system to damage. *Annu. Rev. Neurosci.* **32**, 1–32 (2009).
32. Bowersox, S.S. *et al.* Selective N-type neuronal voltage-sensitive calcium channel blocker, SNX-111, produces spinal antinociception in rat models of acute, persistent and neuropathic pain. *J. Pharmacol. Exp. Ther.* **279**, 1243–1249 (1996).
33. Altier, C. & Zamponi, G.W. Targeting Ca^{2+} channels to treat pain: T-type versus N-type. *Trends Pharmacol. Sci.* **25**, 465–470 (2004).
34. Scott, D.A., Wright, C.E. & Angus, J.A. Actions of intrathecal omega-conotoxins CVID, GVIA, MVIIA, and morphine in acute and neuropathic pain in the rat. *Eur. J. Pharmacol.* **451**, 279–286 (2002).
35. Matthews, E.A. & Dickenson, A.H. Effects of spinally delivered N- and P-type voltage-dependent calcium channel antagonists on dorsal horn neuronal responses in a rat model of neuropathy. *Pain* **92**, 235–246 (2001).
36. Malmberg, A.B. & Yaksh, T.L. Effect of continuous intrathecal infusion of omega-conopeptides, N-type calcium-channel blockers, on behavior and antinociception in the formalin and hot-plate tests in rats. *Pain* **60**, 83–90 (1995).
37. Saegusa, H., Matsuda, Y. & Tanabe, T. Effects of ablation of N- and R-type Ca(2+) channels on pain transmission. *Neurosci. Res.* **43**, 1–7 (2002).
38. Hille, B. *et al.* Multiple G-protein-coupled pathways inhibit N-type Ca channels of neurons. *Life Sci.* **56**, 989–992 (1995).
39. Tedford, H.W. & Zamponi, G.W. Direct G protein modulation of Cav2 calcium channels. *Pharmacol. Rev.* **58**, 837–862 (2006).
40. Elmslie, K.S. Neurotransmitter modulation of neuronal calcium channels. *J. Bioenerg. Biomembr.* **35**, 477–489 (2003).
41. Kammermeier, P.J., Ruiz-Velasco, V. & Ikeda, S.R. A voltage-independent calcium current inhibitory pathway activated by muscarinic agonists in rat sympathetic neurons requires both $G\alpha_{q/11}$ and Gβγ. *J. Neurosci.* **20**, 5623–5629 (2000).
42. Shapiro, M.S. & Hille, B. Substance P and somatostatin inhibit calcium channels in rat sympathetic neurons via different G protein pathways. *Neuron* **10**, 11–20 (1993).
43. Luebke, J.I. & Dunlap, K. Sensory neuron N-type calcium currents are inhibited by both voltage-dependent and -independent mechanisms. *Pflugers Arch.* **428**, 499–507 (1994).
44. Ikeda, S.R. & Dunlap, K. Calcium channels diversify their signaling portfolio. *Nat. Neurosci.* **10**, 269–271 (2007).
45. Ikeda, S.R. & Dunlap, K. Voltage-dependent modulation of N-type calcium channels: role of G protein subunits. *Adv. Second Messenger Phosphoprotein Res.* **33**, 131–151 (1999).
46. Zhang, C. *et al.* Defining the regulatory network of the tissue-specific splicing factors Fox-1 and Fox-2. *Genes Dev.* **22**, 2550–2563 (2008).
47. Licatalosi, D.D. *et al.* HITS-CLIP yields genome-wide insights into brain alternative RNA processing. *Nature* **456**, 464–469 (2008).
48. Boutz, P.L. *et al.* A post-transcriptional regulatory switch in polypyrimidine tract-binding proteins reprograms alternative splicing in developing neurons. *Genes Dev.* **21**, 1636–1652 (2007).
49. Silverman, J.D. & Kruger, L. Selective neuronal glycoconjugate expression in sensory and autonomic ganglia: relation of lectin reactivity to peptide and enzyme markers. *J. Neurocytol.* **19**, 789–801 (1990).
50. Nagy, J.I. & Hunt, S.P. Fluoride-resistant acid phosphatase-containing neurones in dorsal root ganglia are separate from those containing substance P or somatostatin. *Neuroscience* **7**, 89–97 (1982).

ONLINE METHODS

Construction of genomic clones for mouse exon substitution. To create *Cacna1b*$^{b*b/b*b}$ mice, we substituted e37a with e37b*; to create *Cacna1b*$^{aa*/aa}$ mice, we substituted e37b with e37a*. We derived mouse genomic DNA for all constructs from the MICER clone MHPN59f07 (Wellcome Trust Sanger Institute). Details of the cloning steps are given in **Supplementary Methods**. To facilitate detection of the specific exons spliced into the final mRNA products, we introduced silent mutations into restriction sites of the substituted exons; we mutated the BsrGI site in the mutant e37a to produce e37a* and mutated the XhoI site in e37b to produce e37b*.

We inserted a 2-kilobase (kb) *loxP-Neo*^{R}*-loxP* cassette into each targeting construct at the AfeI site located in the intron between the normal positions of e37a and e37b. We added flanking AfeI sites to the *loxP-Neo*^{R}*-loxP* cassette amplified from *PL452* by PCR with primers SD29for and SD31rev. Finally, we reintroduced the mutagenized DNA into BamHI-EagI sites to create the final ~12-kb targeting constructs in pBSSK+.

Mouse embryonic stem cell gene targeting and mouse breeding. Animal housing and experimental procedures were in accordance with Brown institutional animal care and use committee guidelines. In brief, we used 129Ola embryonic stem cells derived from a male embryo, grown on mitotically inactive SNL76/7 feeder cells. We transformed 10^7 embryonic stem cells with 20 µg of a construct linearized with PvuI and selected with G418 after 24 h. We selected 200 G418-resistant clones for further analysis. We used PCR to identify correctly targeted embryonic stem cell clones. We isolated E3.5 blastocysts from C57BL/6- *Tyr*$^{c\text{-}Brd}$ female mice and injected them with 12–20 embryonic stem cells harvested by trypsinization from 90%-confluence cultures. We then implanted injected blastocysts into day-2.5 pseudopregnant females to generate chimeras (eight to ten injected embryos per uterine horn). We mated male chimeras with C57BL/6-*Tyr*$^{c\text{-}Brd}$ females to obtain F1 progeny. We obtained germline transmission of the mutant alleles with several targeted cell lines for each construct.

Identification of correctly targeted embryonic stem cell clones. We confirmed homologous integration with two PCR reactions on genomic DNA from each embryonic stem cell clone. Integration from the long arm was confirmed by PCR amplification of a 7-kb product with Clontech's Advantage 2 Polymerase Mix (35 cycles, 68 °C annealing, 8 min extension at 68 °C) with primers SD77for (anneals 5′ to e37a, outside of the targeting construct sequence) and SD64rev (anneals to the 5′ end of the *Neo*^{R} insert). Homologous integration from the short arm was confirmed by PCR amplification of a 3.5-kb product using Taq polymerase (35 cycles, 60 °C annealing, 4 min extension at 72 °C; New England Biolabs) and primers SD47for (anneals to the 3′ end of the *Neo*^{R} insert) and SD79rev (anneals 3′ to e37b, outside of the targeting construct sequence). We also confirmed correct targeting by sequencing through the substituted region of the *Cacna1b* gene of *Cacna1b*$^{aa*/aa}$ and *Cacna1b*$^{b*b/b*b}$ mice.

We used BsrGI to identify the exon present in the normal e37a position. In BsrGI digests of PCR products amplified using primers SD62for (anneals upstream of the normal e37a position) and SD64rev (35 cycles, 60 °C annealing, 2 min extension at 72 °C with Taq polymerase), e37a was digested by BsrGI (617 and 1,156 bp), whereas e37b* was not (uncut, 1,773 bp). Similarly, we used XhoI to identify the exon present in the normal e37b position, digesting PCR products amplified using primers SD47for and SD48rev (anneals downstream of the normal e37b position). E37b has two XhoI sites (generating products of 144, 216 and 636 bp), and e37a* has one XhoI site (generating products of 144 and 852 bp).

***Neo*^{R} cassette deletion.** We genotyped F1 animals with genomic DNA from tails, using the four primer sets described above. We crossed more than eight positive animals identified for each of the two mutations with a *Cre* deletor strain (B6.FVB-Tg(EIIa-cre)C5379Lmgd/J; Jackson Laboratory stock no. 003724) to delete the *Neo*^{R} gene. We genotyped *ΔNeo*^{R} mice for appropriate e37 mutations (see genotyping below). We crossed *ΔNeo*^{R} siblings carrying appropriate mutations to produce homozygotes that were maintained by crossing of sibling homozygotes. We maintained at least two separate homozygous lines for each mutation.

Genotyping. We used primers SD62for and SD64rev to genotype for *ΔNeo*^{R} by genomic PCR. We performed this genotyping for at least two generations. Refer to **Supplementary Figure 1** for complete genotyping of *Cacna1b*^{ab}, aa* and b*b heterozygotes and homozygotes.

Genomic DNA isolation, RNA extraction and reverse-transcription PCR. See **Supplementary Methods.**

Western blot analysis. We pooled DRG from five mice but carried out three separate experiments on brains from three mice (2–8 months). Details of protein isolation and antibody staining are given in **Supplementary Methods**. We developed all membranes with ECL reagent (Amersham Biosciences) and used time-series exposures to ensure the signal was in the linear range. We measured signal densities (ImageQuantTM software, Amersham) from TIFF images generated from nonsaturated films. After background correction, we quantified $Ca_V2.1$- or $Ca_V2.2$-derived signals as a fraction of the average GAPDH signal. Complete uncropped blots are shown in **Supplementary Figure 5**.

Cell isolation and electrophysiology. We harvested DRG from P7–P9 mice of all three genotypes. We obtained a higher yield of neurons from DRG of these young animals. However, we also recorded N-type currents from mice of the same age as those used for behavior studies (>2 months). Although the yield of neurons was lower from the older mice, we confirmed that results from N-type currents recorded from their nociceptors, for all three genotypes, were not different from those of P7–P9 animals. Single neurons were dissociated from ganglia in Hank's Balanced Salt Solution (HBSS, GIBCO) medium containing 1.5 mg ml^{-1} collagenase (Sigma) and 2 mg ml^{-1} trypsin (Sigma) at 37 °C for ~30 min, then triturated with a fire-polished pipette. We quenched protease activity with Dulbecco's Modified Eagle Medium (DMEM, GIBCO) with 10% fetal bovine serum (vol/vol, FBS, GIBCO). After two washes, we plated neurons on coverslips coated with poly-D-lysine (Sigma) in 10% FBS-DMEM supplemented with 1 ng ml^{-1} nerve growth factor (Sigma) and incubated them at 37 °C with 5% CO_2. We sylgard-coated and fire-polished electrodes to a resistance of 3–6 MΩ. Our external solution contained 135 mM TEA-Cl, 1 mM $CaCl_2$, 10 mM HEPES, 4 mM $MgCl_2$ and 0.1 µM TTX, adjusted to a pH of 7.2 with TEA-OH. Our pipette solution contained 126 mM CsCl, 4 mM Mg-ATP, 1 mM EDTA, 10 mM EGTA and 10 mM HEPES, adjusted to a pH of 7.2 with CsOH. We did not include GTP in the patch pipette because we had evidence from studies of expressed channels[7] that low levels of GTP (0.2–0.3 mM) can lead to tonic inhibition of N-type currents in a voltage-independent manner in the absence of agonist. However, we obtained highly reproducible inhibition of N-type currents by brief repeat applications of DAMGO (Sigma), suggesting that the components necessary for mediating inhibition do not wash out under the conditions of our experiments. We limited the cell's exposure to DAMGO to 1 min. This also avoided µ-opioid receptor desensitization. We evoked whole-cell calcium currents by 10-ms test pulses from a holding potential of −80 mV and monitored tail currents with a 5-ms repolarizing pulse to −60 mV. We applied 2 µM ω-conotoxin GVIA (Alomone) via a pipette to inhibit the N-type current and reapplied voltage steps. We removed ω-conotoxin GVIA from the recording chamber between recordings by washing with 2% SDS (wt/vol) and 10 mM DTT for 20 min. We used pClamp version 8.1 software and the Axopatch 200A (Axon Instruments) for data acquisition; data were filtered at 2 kHz (−3 dB) and sampled at 20 kHz. We compensated series resistance by 70–90% with a 7-µs lag and performed online leak correction with a P/−4 protocol. All recordings were obtained at room temperatures.

Immunofluorescence imaging. Adult mice were deeply anesthetized with intraperitoneal injection of 2% Pentothal (wt/vol), perfused transcardially with 0.9% saline solution (wt/vol) followed by 4% paraformaldehyde (PFA, wt/vol). Spinal cord was removed, post-fixed overnight in 4% PFA, and cryoprotected in 30% sucrose. For comparison, tissues from the three genotypes were frozen and sectioned (20 µm). Sections were dried at room temperature, hydrated in 0.01 M PBS for 15 min and then blocked with 10% goat serum (vol/vol), 0.1% bovine serum albumin (wt/vol) and 0.3% Triton (vol/vol) in PBS in a humidified chamber at room temperature for 1 h. Sections were incubated with 1:200 rabbit anti-$Ca_V2.2$ or 1:800 guinea pig anti-calcitonin gene-related peptide (CGRP) antibodies (Penninsula Labs) overnight at 4 °C. After washing in PBS three times, sections were exposed to Alexa 555–conjugated goat

anti-rabbit IgG (Invitrogen) for $Ca_V2.2$ at room temperature for 2 h. To colabel CGRP and IB4, 1:100 Cy5-conjugated goat anti–guinea pig IgG (Abcam) and 1:100 FITC-conjugated IB4 (Invitrogen) were applied together for 2 h at room temperature. After washing, sections were mounted with Vectashield (Vector labs). Three separate specificity controls were performed. We incubated sections with antigenic peptide preabsorbed with primary antibody, we omitted the primary antibody and we tested $Ca_V2.2$ antibodies on tsA201 cells transfected with $Ca_V2.1$ or mock transfected; we did not observed staining under any of the listed conditions. Polyclonal antibodies to $Ca_V2.1$ and $Ca_V2.2$ were from Alomone labs, and we carried out the following controls to test their specificity. (i) Because $Ca_V2.1$ and $Ca_V2.2$ are relatively similar, we used clones expressed in tsA201 cells to show that anti-$Ca_V2.1$ did not cross-react with $Ca_V2.2$, and likewise that anti-$Ca_V2.2$ did not cross react with $Ca_V2.2$. In addition, we observed no signals in transfections lacking $Ca_V2.1$ and $Ca_V2.2$, either from western blotting or immunofluorescence. (ii) All signals were lost when we omitted the primary antibody and tested with the secondary antibody alone. (iii) Immunofluorescence signals were lost completely in sections in which we first preabsorbed with $Ca_V2.2$ antigenic peptide (**Fig. 6**). Details of the immunofluorescence signals are provided in **Supplementary Methods**.

Behavioral analyses. We tested paw-withdrawal thresholds with Plantar Testing Instruments (IITC)[27] on 8- to 16-week-old male mice. We applied a high-intensity beam (set at 20%, ~45 W) to the middle of the plantar surface of a resting mouse. Paw-withdrawal latency was measured to the nearest 0.1 s, with a cutoff value of 20 s. We injected 3 μg morphine sulfate in a volume of 5 μl intrathecally under anesthesia (2% isoflurane, vol/vol) with a 28-gauge needle connected to a microsyringe through a PE 50 polyester catheter (15 cm)[28]. We tested paw-withdrawal thresholds before and 10, 20, 30, 40, 50 and 60 min after morphine injection. We calculated the percentage of maximum possible effect of morphine (%MPE) using the following formula: $\%MPE = (PWL_{morphine} - PWL_{baseline})100/(20 - PWL_{baseline})$, where PWL is paw-withdrawal latency. We used the area under the curve of %MPE to compare the overall effect of intrathecal morphine among the three genotypes. Data shown in figures are means ± s.e.m. of measurements from at least ten animals for each genotype.

Statistical analysis. Data are presented as means ± s.e.m. Comparisons of mean differences between groups were made by unpaired two-tailed Student's *t*-test unless otherwise stated. $P < 0.05$ was considered to be statistically significant. We used the software Origin 6.1.

doi:10.1038/nn.2643